Direct Synthesis of Novel $Cu_{2-x}Se$ Wurtzite Phase

Emil A. Hernández-Pagán,[∫Δ‡†] Evan H. Robinson,[∫Δ‡] Andrew D. La Croix,[∫Δ†] and Janet E. Macdonald*[∫Δ]

[∫]Department of Chemistry, [Δ]The Vanderbilt Institute of Nanoscale Science and Engineering, Vanderbilt University, Nashville, Tennessee 37235, United States

*Email: janet.macdonald@vanderbilt.edu

KEYWORDS: phase control, nanocrystals, copper selenide, wurtzite, organochalcogenide

ABSTRACT: Herein, we report the unprecedented direct synthesis of a recently discovered metastable wurtzite phase of $Cu_{2-x}Se$. Nanocrystals of $Cu_{2-x}Se$ were synthesized employing dodecyl diselenide as the selenium source and ligand. Optical characterization performed with UV-vis-NIR spectroscopy in solution showed a broad plasmonic band in the NIR. Structural characterization was performed with XRD and TEM. Variable temperature XRD analysis revealed the wurtzite nanocrystals irreversibly transform into the thermodynamic cubic phase at 151°C. Replacement of dodecyl diselenide with dodecyl selenol yielded cubic phase $Cu_{2-x}Se$, allowing for polymorphic phase control. An aliquot study was performed in order to gain insight into the mechanism of phase selectivity. The direct synthesis of this novel wurtzite phase could enable the discovery of new phenomena and expand the vast application space of Cu_xSe_y compounds.

1. INTRODUCTION

The phase of a material is critical in determining the properties exhibited. For example, wurtzite and rock salt CdSe have a direct and indirect band gap, respectively.[1] Similarly, PbO-type FeSe exhibits superconductivity while the NiAs-type does not.[2] However, phase control in the synthesis of polymorphic systems, in particular access to metastable phases, remains a challenge and is the focus of intense research efforts.[3–10] The $Cu_{2-x}Se$ (x=0-0.2) system is of particular interest because this p-type direct band gap semiconductor can exhibit plasmonic properties, superionic conductivity and low thermal conductivity based on composition.[11–14] These characteristics make this material ideal for applications in solar energy, bioimaging,[15] optoelectronics,[13,16] and thermoelectrics.[17]

Controlling the structure of $Cu_{2-x}Se$ (x=0-0.2) in synthesis presents a challenge because the Cu-Se phase diagram is compositionally rich and additionally includes Cu_3Se_2, CuSe, and $CuSe_2$. Furthermore, bulk and nanoscale $Cu_{2-x}Se$ have been reported to crystallize in monoclinic, tetragonal, orthorhombic, and cubic crystal systems.[12,14,17–19] Recently Gariano et al. synthesized hexagonal Cu_2Se with the wurtzite phase via cation exchange of wurtzite-CdSe with Cu^+.[20] While there is very little known about this novel phase, the anisotropic nature of the crystal system and the high mobility of Cu^+ in copper chalcogenides could enable the discovery of new phenomena and the utilization in applications like those mentioned above. Additionally, wurtzite $Cu_{2-x}Se$ can serve as a host material in cation exchange reactions to access metastable phases of other selenides with unique properties.[21,22]

There have been a few literature reports of direct synthetic control of the crystal structure of Cu_2Se. Liu and coworkers developed a synthetic scheme in which Cu nanowires reacted with TOP:Se yielded tetragonal or cubic phase Cu_2Se based on the reaction temperature.[18] Low et al. employed a solventless thermolysis of a copper(I) phenylselenoate polymer under vacuum or inert atmosphere to obtain orthorhombic or cubic Cu_2Se, respectively.[23] However, the direct synthesis of the hexagonal phase has remained elusive because current reaction schemes rely on Se precursors, such as TOP:Se, ODE:Se, and OLAM:Se, that require temperatures ≥ 180 °C to decompose. The higher temperatures likely facilitate formation of the thermodynamic phase. The use of diorganyl dichalcogenides in nanocrystal synthesis has gained momentum in recent years and notably often at more moderate synthetic temperatures.[5,10,16,24–28] In particular, the Brutchey group has exploited these synthons to yield the metastable hexagonal wurtzite phases of $CuInS_2$, $CuInSe_2$, and Cu_2SnSe_3.[24] Herein, we report the direct synthesis and characterization of metastable hexagonal wurtzite $Cu_{2-x}Se$ employing didodecyl diselenide (DD_2Se_2) as the Se precursor.

2. EXPERIMENTAL SECTION

2.1 Materials. Selenium powder (≥99.5 trace metals basis), 1-bromododecane (97%), formic acid (≥95% reagent grade), anhydrous N,N-dimethylformamide (DMF, 99.8%), tetrahydrofuran (THF, ≥99.9%), and 1-octadecene (ODE, 90% technical grade) were obtained from Sigma Aldrich. Sodium borohydride and hydrochloric acid (ACS Plus) were obtained from Fisher Chemicals. Cu(acac)2 (≥98%) was

obtained from Strem Chemicals. All materials were used as received without additional purification.

2.2. Ligand synthesis. *Synthesis of Didodecyl Diselenide:* $C_{24}H_{50}Se_2$ was synthesized following a previously reported procedure.[29] A 1L three-neck round bottom flask was flushed with argon and maintained under inert atmosphere throughout. 75 ml of deionized H_2O was added, followed by 9.3 g (0.12 mol) of selenium powder. The reaction was stirred and cooled on an ice bath for 10 min. 9.8 g (0.26 mol) of $NaBH_4$ was added portion-wise so that the evolution of hydrogen gas did not cause a rapid increase in temperature. The reaction was then allowed to stir for 20 min. Another 9.3 g (0.12 mol) of selenium powder was added and the reaction was allowed to cool to room temperature followed by an additional 20 min. of stirring at room temperature. The flask was then heated to 70 °C and temperature maintained for 20 min. resulting in a clear dark red solution. The reaction was allowed to cool to room temperature. 1-bromododecane (58.6 g, 0.24 mol) and 280 ml of tetrahydrofuran were added dropwise over 30 min. under vigorous stirring. The reaction was then allowed to react at 50 °C for 18 hours, and then it was cooled to room temperature. The phases were separated. The organic layer was washed once with deionized H_2O, then combined organic layers were washed with brine and dried over $MgSO_4$. The solvent was removed under reduced pressure. The crude produce was recrystallized from heptane and isopropyl alcohol over an ice bath to yield yellow needles. Yield: 53.5%.
^{1}H NMR (400MHz, $CDCl_3$) δ 2.92 (t, 4H, J=7.6 Hz), 1.73 (quint, 4H, J=7.5 Hz), 1.27 (m, 36H), 0.88 (t, 3H, J=7.1 Hz).^{13}C NMR (100 MHz, $CDCl_3$) δ 31.86, 30.93, 30.20, 29.61, 29.58, 29.55, 29.47, 29.30, 29.10, 22.63, 14.04. ^{77}Se NMR (76 MHz, $CDCl_3$) δ 307.7.

Synthesis of Dodecyl Selenol: $C_{12}H_{25}SeH$ was synthesized following a previously reported procedure.[29] A 250 mL three-neck round bottom flask was flushed with argon and maintained under inert atmosphere throughout. To the flask was added selenium powder (4.6 g, 0.06 mol) and sodium borohydride powder (4.5 g, 0.12 mol). Anhydrous ethanol (21 ml) as added slowly to the solution. With 20 min. of stirring, a white/grey solid gradually formed. Anhydrous DMF (100 ml) was slowly added. The reaction turned a rufous color, then gradually turned clear and colorless over 30 min. Formic acid (4.6 ml, 0.125 mol) was then added dropwise and the reaction was allowed to stir for 20 min. 1-bromododecane (12 ml, 0.05 mol) was added slowly to the mixture and the reaction was allowed to stir for 4-6 hours, dependent on completion of reaction as verified by quenched aliquots with TLC. (Note: failure to allow reaction to run to completion results in a mixture of dodecylselenol and dodecyl bromide, which forms an azeotrope during distillation and is otherwise challenging to separate by other common purification methods). The reaction was then hydrolyzed with 100 ml of 10% HCl. 50 ml of H_2O was added to the mixture, and the organic was extracted 3x with 50ml of Et_2O. The combined organics were washed once with 10% HCl and dried over $MgSO_4$. The solvent was removed under reduced pressure. Vacuum distillation produced pure dodecyl selenol. ^{1}H NMR (400MHz, $CDCl_3$) δ 2.58 (q, 2H, J=7 Hz), 1.69 (quint, 2H, J=7.5 Hz), 1.26 (m, 18H), 0.88 (t, 3H, J=7.0 Hz), -0.70 (t, 1H, J=6.8 Hz). ^{13}C NMR (100 MHz, $CDCl_3$) δ 33.95, 31.85, 29.58, 29.57, 29.54, 29.49, 29.45, 29.28, 28.92, 22.62, 17.63, 14.04. ^{77}Se NMR (76 MHz, $CDCl_3$) δ -13.1.

2.3 Nanocrystal syntheses. *Synthesis of hexagonal $Cu_{2-x}Se$ NCs*: Standard Schlenk line techniques were used throughout with N_2 as the inert gas. In a typical synthesis, 1.1 mmol of didodecyl diselenide, 0.5 mmol of $Cu(acac)_2$, and 5 mL of octadecene were mixed in a 25 mL 3-necked flask. The flask was put under vacuum and the temperature was raised to 80 ˚C for 30 min. Then the flask was put under inert atmosphere and the temperature was raised to 155 ˚C for 1 hour. The flask was allowed to cool to room temperature, and the post-reaction mixture was precipitated in acetone three times and resuspended in chloroform.

Synthesis of cubic $Cu_{2-x}Se$ NCs: The same procedure as described for the hexagonal $Cu_{2-x}Se$ NCs was followed except didodecyl selenol was used in place of didodecyl diselenide.

2.4 Instrumentation. Transmission Electron Microscopy (TEM) was performed on a FEI Technai Osiris digital 200 kV S/TEM system. Solution absorption spectra were obtained on a Jasco V-670 UV-Vis-NIR spectrophotometer in tetrachloroethylene. X-ray diffraction (XRD) measurements were done using a Rigaku SmartLab powder X-ray diffractometer with a CuKα (λ = 0.154 nm) radiation source set to 40 kV and 44 mA, and a D/teX Ultra 250 1D silicon strip detector. XRD patterns were acquired using a step size of 0.1 degrees at 1 or 10 degrees per minute. High temperature XRD measurements were performed using a Rigaku Multipurpose High Temperature Attachment and a PTC-EVO temperature controller, with a ramp rate of 2 degrees per minute and a holding time of 2 min. ^{1}H NMR spectra were taken using a Bruker DRX-400 (tuned to 400 MHz) spectrometer. Spectra were calibrated to residual solvent signals of 7.26 ppm in $CDCl_3$. ^{13}C and ^{77}Se NMR spectra were taken using a Bruker DRX-500 (tuned to 100 MHz or 76 MHz for ^{13}C or ^{77}Se, respectively) spectrometer. ^{13}C spectra were calibrated to residual solvent signals of 77.0 ppm in $CDCl_3$.

2.6 Computational Methods. The computational methods performed herein were adapted from the works of Guo et al.[28] and Rhodes et al.[10] Bond dissociation energies were calculated using Gaussian with density functional theory (DFT) and the Boese-Martin Kinetics (BMK) functional. Molecular geometry optimization was performed using the 6-31G(d) basis set and single-point energy calculations were performed using the 6-311G(d,p) basis set.

3. RESULTS AND DISCUSSION

In a typical synthesis, $Cu(acac)_2$ and DD_2Se_2 were mixed in octadecene and heated to 155 °C for 1 hr (see experimental section for details). The reaction mixture was cooled down to room temperature and the nanocrystals were separated by centrifugation and purified by washing with acetone. The reaction temperature was selected based on an observed change from a turbid mixture to an optically clear solution indicative of nanocrystal nucleation. Figure 1 illustrates the powder XRD pattern of the as-synthesized nanocrystals. The diffraction peaks match that of the calculated pattern reported by Gariano et al. that

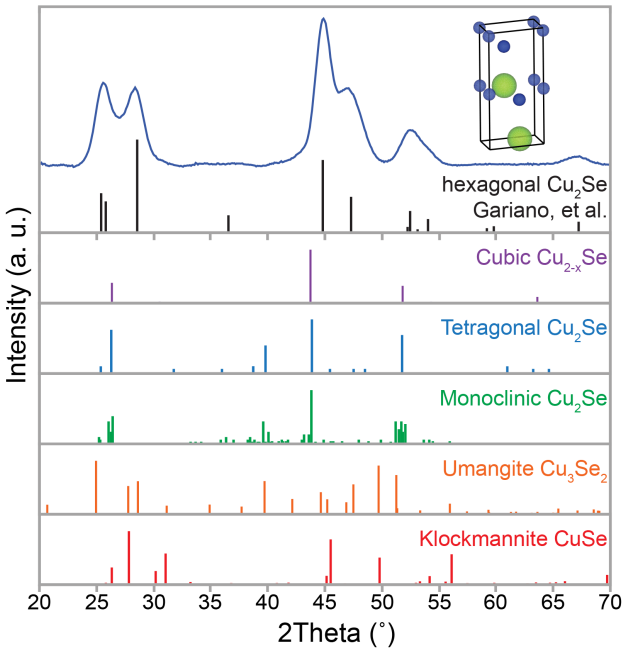

Figure 1. Powder XRD of the wurtzite $Cu_{2-x}Se$ nanocrystals (top), with unit cell and the reference pattern obtained from Gariano, et al., cubic (ICSD: 181661), tetragonal (JCPDS: 29-0575), monoclinic (JCPDS: 27-1131), umangite (ICSD: 16949) and klockmannite (ICSD: 82331) phases of copper selenide.

corresponds to metastable wurtzite $Cu_{2-x}Se$ (space group $P6_3mc$),[20] not those of cubic $Cu_{2-x}Se$, tetragonal and monoclinic Cu_2Se, tetragonal umangite (Cu_3Se_2) and hexagonal klockmannite (CuSe) (Figure 1). Moreover, quantitative energy-dispersive X-ray spectroscopy (EDS) provided a composition close to Cu_2Se (Table S1).

Transmission Electron Microscopy (TEM) analysis revealed the $Cu_{2-x}Se$ nanocrystals have a disk morphology (Figure 2) with an average diameter of 13.8 ± 1.0 nm. Further examination with high-resolution TEM (HR-TEM) and fast Fourier transform (FFT) of the images (Figures S1A-B) reveal an anisotropic crystal structure with the hexagonally close-packed layers stacked along the c-axis. The selected area electron diffraction (SAED) in Figure S2 is consistent with the XRD data.

Based on the bulk Cu-Se phase diagram, berzelianite (cubic)

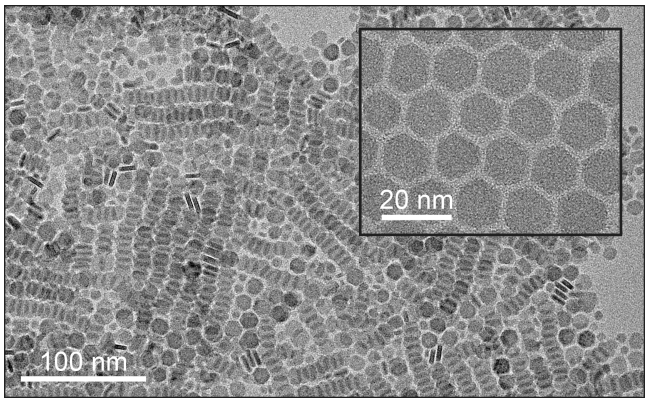

Figure 2. TEM images of $Cu_{2-x}Se$ nanocrystals. A. Disk-shaped NCs aligned in rows. Inset: hexagonal morphology highlighted with close-packed NCs.

$Cu_{2-x}Se$ ($0 < x \leq 0.2$) is the thermodynamic phase in the copper-rich region at temperatures below 1000 K.[30] Although the effects of surface energy and ligands in nanoscale materials can alter the phase diagram, it has been shown that synthesized monoclinic and tetragonal Cu_2Se nanocrystals transform to berzelianite $Cu_{2-x}Se$ upon exposure to air.[12,14] In those systems, oxidation of copper and conversion to the thermodynamic substoichiometric $Cu_{2-x}Se$ phase are closely related and occur in concert. Copper migration from the NC core to the surface accounts for the stoichiometric "loss" of oxidized Cu in the cubic phase (however, the precise location of Cu^{2+} may not be known, and could remain in the core after oxidation[31]). This oxidation results in an increase of charge carrier density giving rise to a plasmon band in the NIR region.[12,14,31] The synthesized nanocrystals were purified under ambient conditions, thus one could expect to see this plasmon band.

Optical characterization was performed by UV-Vis-NIR spectroscopy in solution. The absorbance spectrum is shown in Figure 3. Interestingly, the absorbance spectrum does not exhibit a significant plasmon band in the NIR region. One week of exposure to ambient conditions was required for a broad plasmon band centered at 1900 nm to develop. This is in contrast to observations by Dorfs et al. where cubic $Cu_{1.96}Se$ nanocrystals exhibited a plasmon band at ~ 1600 nm after one minute under ambient conditions.[32] Similarly, Kriegel et al. observed the emergence of an intense plasmon band in the spectral region *ca* 1300-1400 nm as tetragonal Cu_2Se nanocrystals oxidized to cubic $Cu_{1.8}Se$ within 5.5 hrs.[14] The red shifted plasmon band observed here suggests a composition close to stoichiometry Cu_2Se, in agreement with the EDS results (Table S1). Furthermore, the relatively slow formation of a NIR surface plasmon and its position indicate that our synthetic conditions and ligand environment yield nanocrystals that are only weakly susceptible to oxidation. It should be noted the wurtzite $Cu_{2-x}Se$ NCs remained in the hexagonal crystal structure and with similar mor-

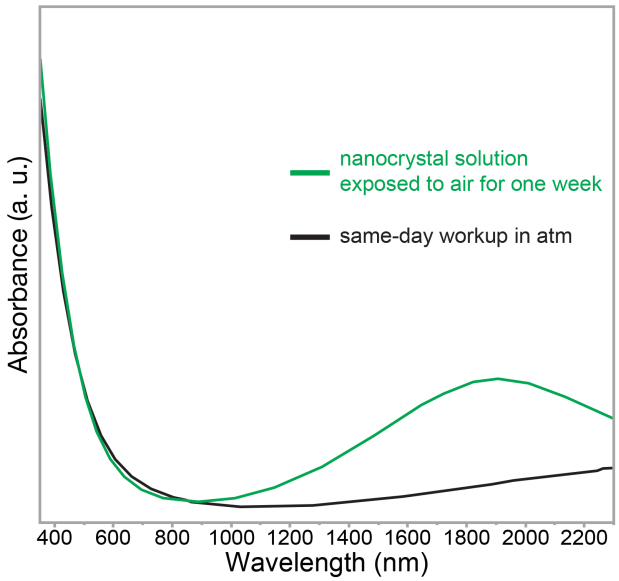

Figure 3. UV-vis-NIR spectra of wurtzite $Cu_{2-x}Se$ nanocrystals after the work up and after one week of storage, both under ambient conditions.

phology after weeks of air exposure (Figure S3 and S4).

In light of the prolonged stability of the hexagonal phase of the nanocrystals, variable temperature XRD was employed to force a phase transition at elevated temperatures. Data in Figure 4A shows XRD patterns collected from 37 ˚C to 186 ˚C with some key features. Diagnostic of the phase change, the reflection corresponding to the (111) plane of berzelianite $Cu_{2-x}Se$ emerges as the temperature increases at the expense of the (002), (100) and (101) reflections of the wurtzite structure. Following the work of Rivest et al.,[33] phase transition temperature was calculated by fitting a Boltzmann function to the integrated intensity of the diminishing wurtzite peak at 25.2˚. As depicted in Figure 4B, the transition temperature from the wurtzite to berzelianite crystal structure was found to be approximately 151 ˚C. To verify the transition temperature, the synthesized nanocrystals were heated in octadecene at 150 ˚C for 1 hr; as was

expected the nanocrystals transformed into the berzelianite (cubic) phase (Figure S5).

The transition temperature being close to the synthesis temperature highlights the advantage of regents active at moderate temperatures. Reaction aliquots taken below 155°C showed no evidence of nanocrystal formation, yet a distinct color change from blue to brown was observed at 155°C as nanocrystals formed. Control syntheses performed at 165 ˚C and 175 ˚C yielded predominantly wurtzite nanocrystals but with phase impurities (Figure S6). At 185 ˚C, berzelianite $Cu_{2-x}Se$ nanocrystals were obtained. It appears the reactivity of DD_2Se_2 is at a bare minimum to achieve the phase purity of the metastable phase observed. A reagent any less reactive and requiring higher reaction temperatures or longer times would have resulted in significant impurities of the thermodynamic cubic phase.

Given this low transition temperature, the direct synthesis of wurtzite $Cu_{2-x}Se$ was in part achievable because of the moderate reaction temperature facilitated by the facile decomposition of DD_2Se_2. A reagent any less reactive and requiring higher reaction temperatures would have resulted in significant impurities of the thermodynamic cubic phase.

To test if the lower reaction temperature was the only factor responsible for the formation of the wurtzite phase, DD_2Se_2 was replaced with dodecylselenol (DDSeH). When DDSeH was used under otherwise identical conditions, the reaction yields the thermodynamic product, berzelianite $Cu_{2-x}Se$ (Figure S7) instead of the wurtzite product. Previous literature reports have shown control of the product phase when using dialkyl dichalcogenides with different substituents and with dialkyl dichalcogenides vs alkyl thiol/selenol.[10,24] The phase control has been attributed in part to the relative strength of the C-X and X-X (X=Se, S) bonds, and consequently the chalcogenide transfer rate. More easily cleaved bonds in the organochalcogenide lead to the thermodynamic products. For example, in the synthesis of $CuInSe_2$, Tappan et al.[25] were able to selectively obtain the thermodynamic chalcopyrite or the metastable wurtzite $CuInSe_2$ product employing dibenzyl diselenide (C-Se 43 kcal/mol) or diphenyl diselenide (C-Se 65 kcal/mol), respectively, as the Se source. Similarly, the copper selenide intermediates of these reactions showed a similar trend. The reaction progressed through the thermodynamically stable intermediates of berzelianite $Cu_{2-x}Se$ and klockmannite CuSe when dibenzyl

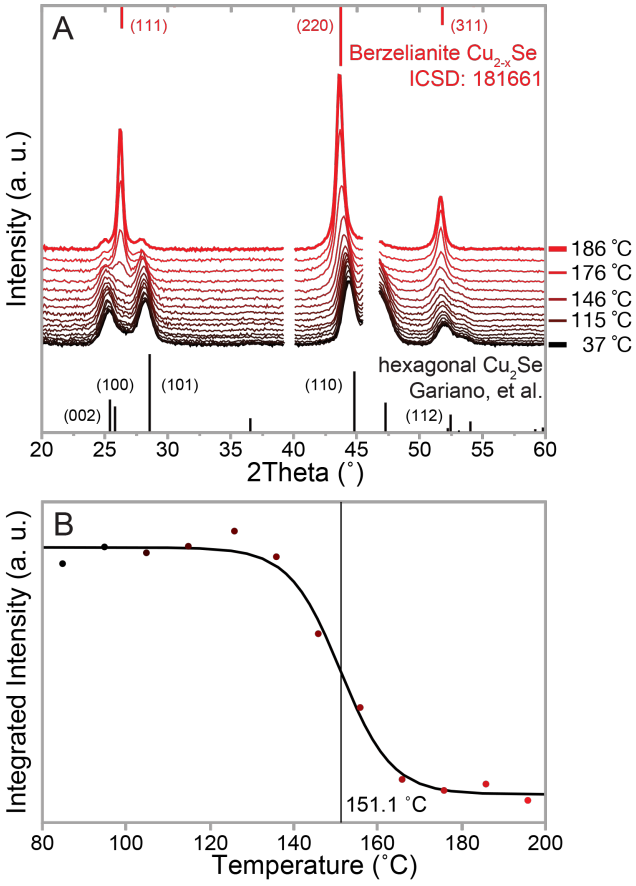

Figure 4. A. Variable temperature powder XRD of wurtzite $Cu_{2-x}Se$ nanocrystals along with the reference patterns for wurtzite and berzelianite $Cu_{2-x}Se$. Platinum reflections at 39.8˚ and 46.2˚ due to the sample holder have been omitted. B. The cubic 25.2˚ reflections were integrated and plotted versus temperature to calculate the phase transition temperature of 151 ˚C per Rivest et al.

or dimethyl diselenide (weaker C-Se bonds) were employed. Conversely, reactions involving diphenyl diselenide (stronger C-Se bonds) progressed via the metastable intermediate umangite Cu_3Se_2.

DFT calculations (Figure S8) revealed C-Se bond strengths of 55.4 kcal/mol and 67.8 kcal/mol for DD_2Se_2 and DDSeH,

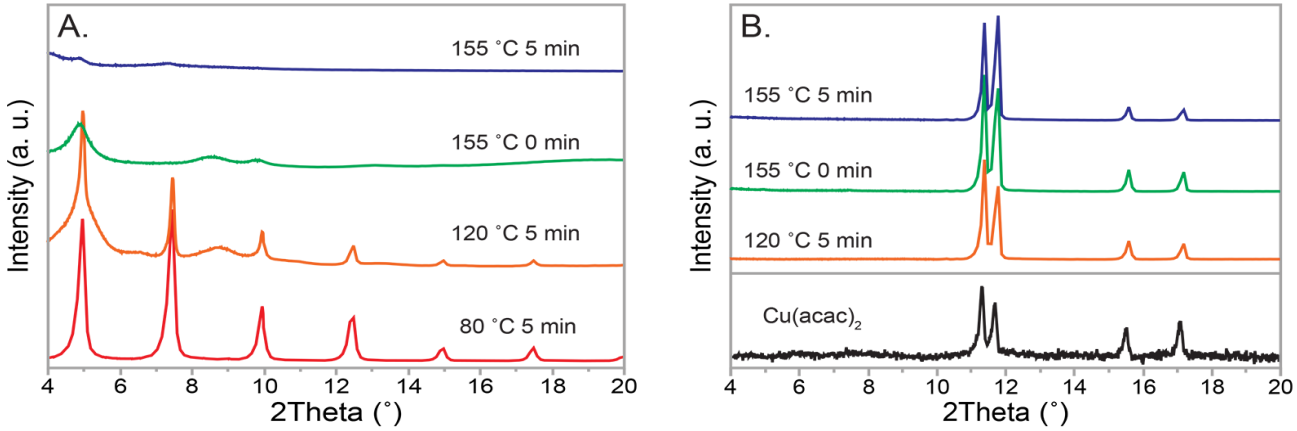

Figure 5. Aliquot XRD study of the precursor formation during $Cu_{2-x}Se$ syntheses. A. When dodecaneselenol is used in a NC synthesis, the selenol reacts with Cu early on in the heat-up to reaction temperature of 155 ˚C, generating a lamellar mesophase similar to that observed by Bryks, et al. results with Cu_2S. B. Didodecane diselenide shows less reactivity during the heat-up and only $Cu(acac)_2$ is detected with XRD.

respectively, following the same trend as previously reported for other organochalcogenides. Given the above hypothesis, one would expect the DD_2Se_2 to give the thermodynamic phase and DDSeH to give the metastable phase, yet the results here are the opposite. Therefore, other factors are at play.

To shed some light on the mechanistic details that lead to phase control, aliquots of the reactions taken at 80 °C, 120 °C, 0 min@155 °C, and 5 min@155 °C were analyzed with XRD. Figure 5A shows the patterns for the syntheses with DDSeH. The XRD pattern for the 80 °C aliquot reveals the formation of a Cu-selenoate complex ($CH_3(CH_2)_{10}CH_2Se$-Cu). This complex was also observed in the work of Bryks et al.[27] and Berends et al.[26] This Cu-selenoate complex is a lamellar mesophase analogous to the well documented metal-thiolate complexes, which have been exploited in the synthesis of metal and metal sulfide nanocrystals.[34–36] The reflections corresponding to the complex remained present at 120 °C, yet subsided significantly when the system reached the reaction temperature (0 min@155 °C). After 5 min at 155 °C, the complex was no longer present, indicative of the nucleation onset of $Cu_{2-x}Se$. In contrast, for DD_2Se_2 (Figure 5b), the XRD patterns of the four corresponding aliquots early in the reaction sequence matched the reflections for $Cu(acac)_2$. The presence of the diselenide bond prevents formation of the Cu-selenoate complex as presumably a homolytic cleavage of the Se-Se bond would be required as opposed to a simple ligand exchange.

In the context of the previous observations of others of phase control based on bond strength of the precursors, we posit that the formation of the complex results in Cu withdrawing electron density from Se, weakening the C-Se bond for the DDSeH. Since the copper-thiolate complex does not readily form as an intermediate for DD_2Se_2, this reagent is the less reactive of the two. Thus, in agreement with the previous observations in the literature, the more-reactive precursor leads to the thermodynamically favored cubic phase under synthetic conditions.

It is known that ligands can direct the phase of the products in other metal-chalcogenide systems,[9,10,37] and the copper selenide system is similarly susceptible. As mentioned earlier, a Cu-selenoate complex was observed to form in the work by Bryks et al.[27] and Berends et al.,[26] however these two reactions yielded different products. The solventless thermolysis of a Cu-selenoate complex performed by Bryks et al. formed the thermodynamic product, berzelianite $Cu_{2-x}Se$. This system is similar to ours, but without the non-coordinating solvent octadecene present in our reaction, which facilitates the diffusion of reactants. In contrast, the reaction system employed by Berends et al. contained additional ligands (e.g. trioctylphosphine oxide, oleylamine) and lead to nanocrystals of umangite Cu_3Se_2. Similarly, Tappan et al. observed umangite Cu_3Se_2 *en route* to wurtzite $CuInSe_2$ in the presence of oleic acid and oleylamine. Care must therefore be taken when comparing results with differing ligands present. The reaction system in the present work was intentionally simplified by utilizing a non-coordinating solvent, and DD_2Se_2 or DDSeH as both the selenium source and ligands.

Ligands may play unrecognized roles in the decomposition mechanism of the organochalcogenide reactants. Our lab has shown, for example, that oleylamine plays a key role in the decomposition of allyl disulfide.[10] Similarly, the Hogarth group recognized amines were changing the reactive organometallic intermediate decomposition mechanism of nickel dithiocarbamates, influencing the phase of the resultant nickel sulfide.[38] Ligands may also alter the surface energies of the growing nuclei,[37] and our group has previously shown that thiol sulfur precursors, can provide highly bridged surfaces chemistries of the thiol ligands.[39,40] Further work in the corresponding organoselenide chemistry is in progress.

4. CONCLUSION

In summation, a direct synthesis for the recently discovered copper(I) selenide wurtzite phase was developed using didodecyl diselenide as a nanocrystal selenium source and ligand. XRD confirmed the hexagonal phase initially discovered by Gariano, et al., and TEM revealed a platelet-like morphology. A high-temperature study showed that the metastable wurtzite phase converted to the thermodynamic berzelianite phase at approximately 151 ˚C. DDSeH alternatively provided the cubic Cu_2Se product, through a copper selenoate intermediate with a hypothesized weaker C-Se bond than DD_2Se_2. The synthesis of other metal selenides with DD_2Se_2 and DDSeH as ligands/selenium source is currently in progress, as well as an investigation into how the additional ligands (e.g. TOP) alter the resulting phase as previously observed by others.

ASSOCIATED CONTENT

Supporting Information. The Supporting Information is available free of charge on the ACS Publications website.

Additional characterization: XRD, TEM, SAED, EDS. (PDF)

AUTHOR INFORMATION

Corresponding Author

* janet.macdonald@vanderbilt.edu

Present Addresses

† E.A.H.-P. current address: 104 Chemistry Building, Penn State University, University Park, PA 16801 USA.

A.D.L. current address: Department of Chemistry, Lander University, 320 Stanley Avenue, Greenwood, SC 29649 USA

Author Contributions

‡These authors contributed equally.

Note

The authors declare no competing financial interest.

ACKNOWLEDGMENT

This work was financially supported by NSF grant EPS-1004083 and the Vanderbilt Institute of Nanoscale Science and Engineering. EHR thanks and acknowledges support from the Mitchum E. Warren Fellowship. The authors thank Ross Koby and Jordan Rhodes for assistance with DFT calculations.

ABBREVIATIONS

DD_2Se_2, didodecyl diselenide; DDSeH, dodecylselenol

REFERENCES

(1) Tolbert, S. H.; Alivisatos, A. P. Size Dependence of a First Order Solid-Solid Phase Transition : The Wurtzite to Rock Salt Transformation in CdSe Nanocrystals. *Science (80).* **1994**, *265*

(5170), 373–376.
(2) Hussain, R. A.; Badshah, A.; Lal, B. Fabrication, Characterization and Applications of Iron Selenide. *J. Solid State Chem.* **2016**, *243*, 179–189.
(3) Fenton, J. L.; Schaak, R. E. Structure-Selective Cation Exchange in the Synthesis of Zincblende MnS and CoS Nanocrystals. *Angew. Chemie - Int. Ed.* **2017**, *56* (23), 6464–6467.
(4) Nam, K. M.; Kim, Y.-I.; Jo, Y.; Lee, S. M.; Kim, B. G.; Choi, R.; Choi, S.-I.; Song, H.; Park, J. T. New Crystal Structure: Synthesis and Characterization of Hexagonal Wurtzite MnO. *J. Am. Chem. Soc.* **2012**, *134* (20), 8392–8395.
(5) Norako, M. E.; Greaney, M. J.; Brutchey, R. L. Synthesis and Characterization of Wurtzite-Phase Copper Tin Selenide Nanocrystals. *J. Am. Chem. Soc.* **2012**, *134* (1), 23–26.
(6) Powell, A. E.; Hodges, J. M.; Schaak, R. E. Preserving Both Anion and Cation Sublattice Features during a Nanocrystal Cation-Exchange Reaction: Synthesis of Metastable Wurtzite-Type CoS and MnS. *J. Am. Chem. Soc.* **2016**, *138* (2), 471–474.
(7) Seo, W. S.; Shim, J. H.; Oh, S. J.; Lee, E. K.; Hur, N. H.; Park, J. T. Phase- and Size-Controlled Synthesis of Hexagonal and Cubic CoO Nanocrystals. *J. Am. Chem. Soc.* **2005**, *127* (17), 6188–6189.
(8) Singh, S.; Ryan, K. M. Occurrence of Polytypism in Compound Colloidal Metal Chalcogenide Nanocrystals, Opportunities, and Challenges. *J. Phys. Chem. Lett.* **2015**, *6* (16), 3141–3148.
(9) Gao, Y.; Peng, X. Crystal Structure Control of CdSe Nanocrystals in Growth and Nucleation: Dominating Effects of Surface versus Interior Structure. *J. Am. Chem. Soc.* **2014**, *136* (18), 6724–6732.
(10) Rhodes, J. M.; Jones, C. A.; Thal, L. B.; MacDonald, J. E. Phase-Controlled Colloidal Syntheses of Iron Sulfide Nanocrystals via Sulfur Precursor Reactivity and Direct Pyrite Precipitation. *Chem. Mater.* **2017**, *29* (19), 8521–8530.
(11) Scotognella, F.; Della Valle, G.; Srimath Kandada, A. R.; Dorfs, D.; Zavelani-Rossi, M.; Conforti, M.; Miszta, K.; Comin, A.; Korobchevskaya, K.; Lanzani, G.; et al. Plasmon Dynamics in Colloidal $Cu_{2-x}Se$ Nanocrystals. *Nano Lett.* **2011**, *11* (11), 4711–4717.
(12) Riha, S. C.; Johnson, D. C.; Prieto, A. L. Cu_2Se Nanoparticles with Tunable Electronic Properties Due to a Controlled Solid-State Phase Transition Driven by Copper Oxidation and Cationic Conduction. *J. Am. Chem. Soc.* **2011**, *133* (5), 1383–1390.
(13) Liu, X.; Wang, X.; Zhou, B.; Law, W. C.; Cartwright, A. N.; Swihart, M. T. Size-Controlled Synthesis of $Cu_{2-x}E$ (E = S, Se) Nanocrystals with Strong Tunable Near-Infrared Localized Surface Plasmon Resonance and High Conductivity in Thin Films. *Adv. Funct. Mater.* **2013**, *23* (10), 1256–1264.
(14) Kriegel, I.; Jiang, C.; Rodríguez-Fernández, J.; Schaller, R. D.; Talapin, D. V.; Da Como, E.; Feldmann, J. Tuning the Excitonic and Plasmonic Properties of Copper Chalcogenide Nanocrystals. *J. Am. Chem. Soc.* **2012**, *134* (3), 1583–1590.
(15) Hessel, C. M.; P. Pattani, V.; Rasch, M.; Panthani, M. G.; Koo, B.; Tunnell, J. W.; Korgel, B. A. Copper Selenide Nanocrystals for Photothermal Therapy. *Nano Lett.* **2011**, *11* (6), 2560–2566.
(16) Wang, W.; Zhang, L.; Chen, G.; Jiang, J.; Ding, T.; Zuo, J.; Yang, Q. $Cu_{2-x}Se$ Nanooctahedra: Controllable Synthesis and Optoelectronic Properties. *CrystEngComm* **2015**, *17* (9), 1975–1981.
(17) Eikeland, E.; Blichfeld, A. B.; Borup, K. A.; Zhao, K.; Overgaard, J.; Shi, X.; Chen, L.; Iversen, B. B. Crystal Structure across the β to α Phase Transition in Thermoelectric $Cu_{2-x}Se$. *IUCrJ* **2017**, *4*, 476–485.
(18) Liu, S.; Zhang, Z.; Bao, J.; Lan, Y.; Tu, W.; Han, M.; Dai, Z. Controllable Synthesis of Tetragonal and Cubic Phase Cu_2Se Nanowires Assembled by Small Nanocubes and Their Electrocatalytic Performance for Oxygen Reduction Reaction. *J. Phys. Chem. C* **2013**, *117* (29), 15164–15173.
(19) Coughlan, C.; Ibáñez, M.; Dobrozhan, O.; Singh, A.; Cabot, A.; Ryan, K. M. Compound Copper Chalcogenide Nanocrystals. *Chem. Rev.* **2017**, *117* (9), 5865–6109.
(20) Gariano, G.; Lesnyak, V.; Brescia, R.; Bertoni, G.; Dang, Z.; Gaspari, R.; De Trizio, L.; Manna, L. Role of the Crystal Structure in Cation Exchange Reactions Involving Colloidal Cu_2Se Nanocrystals. *J. Am. Chem. Soc.* **2017**, *139* (28), 9583–9590.
(21) Beberwyck, B. J.; Surendranath, Y.; Alivisatos, A. P. Cation Exchange: A Versatile Tool for Nanomaterials Synthesis. *J. Phys. Chem. C* **2013**, *117* (39), 19759–19770.
(22) De Trizio, L.; Manna, L. Forging Colloidal Nanostructures via Cation Exchange Reactions. *Chem. Rev.* **2016**, *116* (18), 10852–10887.
(23) Low, K. H.; Li, C. H.; Roy, V. A. L.; Chui, S. S. Y.; Chan, S. L. F.; Che, C. M. Homoleptic Copper(I) Phenylselenolate Polymer as a Single-Source Precursor for Cu_2Se Nanocrystals. Structure, Photoluminescence and Application in Field-Effect Transistor. *Chem. Sci.* **2010**, *1* (4), 515–518.
(24) Brutchey, R. L. Diorganyl Dichalcogenides as Useful Synthons for Colloidal Semiconductor Nanocrystals. *Acc. Chem. Res.* **2015**, *48* (11), 2918–2926.
(25) Tappan, B. A.; Barim, G.; Kwok, J. C.; Brutchey, R. L. Utilizing Diselenide Precursors toward Rationally Controlled Synthesis of Metastable $CuInSe_2$ Nanocrystals. *Chem. Mater.* **2018**, *30* (16), 5704–5713.
(26) Berends, A. C.; van der Stam, W.; Akkerman, Q. A.; Meeldijk, J. D.; van der Lit, J.; de Mello Donega, C. Anisotropic 2D $Cu_{2-x}Se$ Nanocrystals from Dodecaneselenol and Their Conversion to CdSe and $CuInSe_2$ Nanoparticles. *Chem. Mater.* **2018**, *30* (11), 3836–3846.
(27) Bryks, W.; Smith, S. C.; Tao, A. R. Metallomesogen Templates for Shape Control of Metal Selenide Nanocrystals. *Chem. Mater.* **2017**, *29* (8), 3653–3662.
(28) Guo, Y.; Alvarado, S. R.; Barclay, J. D.; Vela, J. Shape-Programmed Nanofabrication: Understanding the Reactivity of Dichalcogenide Precursors. *ACS Nano* **2013**, *7* (4), 3616–3626.
(29) Dilimon, V. S.; Fonder, G.; Delhalle, J.; Mekhalif, Z. Self-Assembled Monolayer Formation on Copper: A Real Time Electrochemical Impedance Study. *J. Phys. Chem. C* **2011**, *115* (37), 18202–18207.
(30) Glazov, V. M.; Pashinkin, A. S.; Fedorov, V. A. Phase Equilibria in the Cu-Se System. *Inorg. Mater.* **2000**, *36* (7), 641–652.
(31) Marbella, L. E.; Gan, X. Y.; Kaseman, D. C.; Millstone, J. E. Correlating Carrier Density and Emergent Plasmonic Features in $Cu_{2-x}Se$ Nanoparticles. *Nano Lett.* **2017**, *17* (4), 2414–2419.
(32) Dorfs, D.; Härtling, T.; Miszta, K.; Bigall, N. C.; Kim, M. R.; Genovese, A.; Falqui, A.; Povia, M.; Manna, L. Reversible Tunability of the Near-Infrared Valence Band Plasmon Resonance in $Cu_{2-x}Se$ Nanocrystals. *J. Am. Chem. Soc.* **2011**, *133* (29), 11175–11180.
(33) Rivest, J. B.; Fong, L.-K.; Jain, P. K.; Toney, M. F.; Alivisatos, A. P. Size Dependence of a Temperature-Induced Solid-Solid Phase Transition in Copper(I) Sulfide. *J. Phys. Chem. Lett.* **2011**, *2*, 2402–2406.
(34) Bryks, W.; Lupi, E.; Ngo, C.; Tao, A. R. Digenite Nanosheets Synthesized by Thermolysis of Layered Copper-Alkanethiolate Frameworks. *J. Am. Chem. Soc.* **2016**, *138* (41), 13717–13725.
(35) Chen, Y. B.; Chen, L.; Wu, L. M. Structure-Controlled Solventless Thermolytic Synthesis of Uniform Silver Nanodisks. *Inorg. Chem.* **2005**, *44* (26), 9817–9822.
(36) Dance, I. G.; Fisher, K. J.; Banda, R. M. H.; Scudder, M. L. Layered Structure of Crystalline Compounds AgSR. *Inorg. Chem.* **1991**, *30* (2), 183–187.
(37) Huang, J.; Kovalenko, M. V.; Talapin, D. V. Alkyl Chains of Surface Ligands Affect Polytypism of CdSe Nanocrystals and Play an Important Role in the Synthesis of Anisotropic Nanoheterostructures. *J. Am. Chem. Soc.* **2010**, *132* (45), 15866–15868.
(38) Hollingsworth, N.; Roffey, A.; Islam, H. U.; Mercy, M.; Roldan, A.; Bras, W.; Wolthers, M.; Catlow, C. R. A.; Sankar, G.; Hogarth, G.; et al. Active Nature of Primary Amines during Thermal Decomposition of Nickel Dithiocarbamates to Nickel Sulfide Nanoparticles. *Chem. Mater.* **2014**, *26* (21), 6281–6292.
(39) Turo, M. J.; Macdonald, J. E. Crystal-Bound vs Surface-Bound Thiols on Nanocrystals. *ACS Nano* **2014**, *8* (10), 10205–10213.
(40) Turo, M. J.; Shen, X.; Brandon, N. K.; Castillo, S.; Fall, A. M.; Pantelides, S. T.; Macdonald, J. E. Dual-Mode Crystal-Bound and X-Type Passivation of Quantum Dots. *Chem. Commun.* **2016**, *52* (82), 12214–12217.

SYNOPSIS TOC (Word Style "SN_Synopsis_TOC"). If you are submitting your paper to a journal that requires a synopsis graphic and/or synopsis paragraph, see the Instructions for Authors on the journal's homepage for a description of what needs to be provided and for the size requirements of the artwork.

To format double-column figures, schemes, charts, and tables, use the following instructions:

Place the insertion point where you want to change the number of columns
From the **Insert** menu, choose **Break**
Under **Sections**, choose **Continuous**
Make sure the insertion point is in the new section. From the **Format** menu, choose **Columns**
In the **Number of Columns** box, type **1**
Choose the **OK** button

Now your page is set up so that figures, schemes, charts, and tables can span two columns. These must appear at the top of the page. Be sure to add another section break after the table and change it back to two columns with a spacing of 0.33 in.

Table 1. Example of a Double-Column Table

Column 1	Column 2	Column 3	Column 4	Column 5	Column 6	Column 7	Column 8

Authors are required to submit a graphic entry for the Table of Contents (TOC) that, in conjunction with the manuscript title, should give the reader a representative idea of one of the following: A key structure, reaction, equation, concept, or theorem, etc., that is discussed in the manuscript. Consult the journal's Instructions for Authors for TOC graphic specifications.

Insert Table of Contents artwork here